PHYSICAL REVIEW A **90**, 042713 (2014)

Electron-loss-to-continuum cusp in $U^{88+} + N_2$ collisions

P.-M. Hillenbrand,[1,2,*] S. Hagmann,[1,3,†] A. B. Voitkiv,[3,4,5] B. Najjari,[6] D. Banaś,[7] K.-H. Blumenhagen,[1,8,9] C. Brandau,[2,10] W. Chen,[1] E. De Filippo,[11] A. Gumberidze,[10,12] D. L. Guo,[13] C. Kozhuharov,[1] M. Lestinsky,[1] Yu. A. Litvinov,[1,4,14] A. Müller,[2] H. Rothard,[15] S. Schippers,[2] M. S. Schöffler,[3] U. Spillmann,[1] S. Trotsenko,[1,8] X. L. Zhu,[13] and Th. Stöhlker[1,8,9]

[1]*GSI Helmholtzzentrum für Schwerionenforschung, D-64291 Darmstadt, Germany*

[2]*Institut für Atom- und Molekülphysik, Justus-Liebig-Universität Giessen, D-35392 Giessen, Germany*

[3]*Institut für Kernphysik, Goethe Universität Frankfurt, D-60438 Frankfurt am Main, Germany*

[4]*Max-Planck-Institut für Kernphysik, D-69117 Heidelberg, Germany*

[5]*Institut für Theoretische Physik I, Heinrich-Heine-Universität Düsseldorf, D-40225 Düsseldorf, Germany*

[6]*Institut Pluridisciplinaire Hubert Curien, Université de Strasbourg, F-67037 Strasbourg Cedex 2, France*

[7]*Institute of Physics, Jan Kochanowski University, PL-25-406 Kielce, Poland*

[8]*Helmholtz-Institut Jena, D-07743 Jena, Germany*

[9]*Institut für Optik und Quantenelektronik, Friedrich-Schiller-Universität Jena, D-07743 Jena, Germany*

[10]*ExtreMe Matter Institute EMMI and Research Division, GSI Helmholtzzentrum für Schwerionenforschung, D-64291 Darmstadt, Germany*

[11]*Istituto Nazionale di Fisica Nucleare Sezione di Catania, I-95123 Catania, Italy*

[12]*FIAS Frankfurt Institute for Advanced Studies, D-60438 Frankfurt am Main, Germany*

[13]*Institute of Modern Physics, Chinese Academy of Sciences, Lanzhou 730000, China*

[14]*Ruprecht-Karls Universität Heidelberg, D-69120 Heidelberg, Germany*

[15]*Centre de Recherche sur les Ions, les Matériaux et la Photonique, CIMAP-CIRIL-Ganil, F-14070 Caen, France*

(Received 16 September 2014; published 27 October 2014)

The electron loss to the continuum has been studied for the collision system $U^{88+} + N_2 \rightarrow U^{89+} + [N_2]^* + e^-$ at the low-relativistic projectile energy of 90 MeV/u. Using a magnetic electron spectrometer, the energy distribution of cusp electrons emitted at an angle of 0° with respect to the projectile beam was measured in coincidence with the up-charged projectile. At the experimental collision energy ionization of the berylliumlike U^{88+} projectile proceeds predominantly from the L shell, but a contribution from the K shell could also be identified experimentally. The measurement is shown to be in accordance with fully relativistic Dirac calculations applying first-order perturbation theory. Furthermore, the underlying continuum electron distribution in the projectile frame is illustrated.

DOI: 10.1103/PhysRevA.90.042713 PACS number(s): 34.50.Fa, 32.80.Hd

I. INTRODUCTION

Our knowledge about the dynamical processes which result in ionization, excitation, and electron transfers in ion-atom collisions has immensely increased since heavy-ion storage rings [1,2] have enabled a more detailed and a considerably refined approach to an experimental differentiation of the various mechanisms producing electron and photon spectra of high yet distinguishing complexity [3–11]. In heavy-ion storage rings collisions of projectiles in charge states ranging up to fully ionized uranium with atomic and molecular gas targets can be studied at relativistic collision energies with unprecedented clean conditions. Typically, the collision systems studied comprise electrons over a wide range of characteristic velocities: for targets with low atomic number Z_t the projectile velocity v_p is significantly higher than the orbital velocities of the electrons in the target atom, $v_p \gg Z_t$ (in atomic units). At the same time the collision velocity may be similar to the orbital velocity of the K-shell electron of the projectile, $v_p \approx Z_p$. When excitation or ionization of the projectile is studied, and the final state of the target atom is not considered, a light target atom can be seen as a weak perturbation for the swiftly passing projectile. As such, experimental studies of these collision systems provide stringent tests for advanced theories describing projectile excitation and ionization of highly charged heavy ions. These theories typically include fully relativistic bound-state and continuum one-electron Dirac wave functions, and first-order perturbation theory for the interaction between the projectile ion and the target atom [12–17].

Various measurements of Coulomb excitation of heavy projectiles in collisions with light target atoms were performed using x-ray spectroscopy, where the final state could be identified through the emitted photon [6,18–20]. In this context, the measurement of the electron-loss-to-continuum cusp corresponds to a projectile ionization, where the final state of the electron is identified by its continuum energy. Corresponding measurements in the low-relativistic regime providing benchmark data for theory were unavailable until now.

From well-established electron spectroscopy experiments performed in single-pass configuration with swift nonbare projectiles, it is known that the highest intensity of the emitted electrons can be observed at an angle of $\vartheta_e \approx 0°$ with respect to the projectile beam [21–23]. Depending on the collision system, electrons with a velocity v_e similar to the projectile velocity v_p (i.e., cusp electrons) may originate from three competing processes with a clearly distinct cusp

*p.m.hillenbrand@gsi.de
†s.hagmann@gsi.de

shape: In the electron capture to continuum (ECC) one or more electrons from the target atom are captured into the projectile continuum [21–35]. In the radiative electron capture to continuum (RECC) [7,8,36,37] an electron from the target atom is captured into the projectile continuum while emitting a photon. Finally, in the electron loss to continuum (ELC) an electron from the projectile is ionized into the projectile continuum during the collision with a target atom [38–45]. Consequently, electrons originating from ELC can be unambiguously identified only by application of a coincidence condition between the observed electron and the up-charged projectile. Although ELC has been observed for several decades, few experimental data from application of this rigorous coincidence technique are available. They include coincidence measurements with light projectiles [46–50], neutral projectiles [51], and multielectron projectiles [21,34,35,52–54]. In particular, measurements of ELC using fast multielectron projectiles revealed complex structures, since some spectra had superimposed Auger electrons arising from double excitation or inner-shell ionization of the projectile. A striking discrepancy was found between measurements of ELC with projectiles at ultrarelativistic energies [55] and current theoretical descriptions [56,57].

Due to the Lorentz transformation electrons ionized from the projectile in these collisions are predominantly emitted into the forward direction with a velocity similar to the projectile velocity [58]. The observation of electrons at a scattering angle of $\vartheta_e \approx 0^\circ$ is advantageous, since the achievable energy resolution is not limited by Doppler broadening within the finite observation angle. For the theoretical calculation of the corresponding electron spectrum, the energy- and angular-differential distribution of the emitted electron is calculated in the projectile frame and transformed into the laboratory frame. Thus, the measured electron spectra provide insight into the ionization mechanisms beyond the studies of absolute ionization cross sections, which have been performed both experimentally [59–64] and theoretically [12,14,15] for these collision systems. Regarding the ionization of few-electron uranium projectiles in collisions with atomic targets there have been several theoretical calculations of double-differential cross sections [17,65,66], but up to now no experimental data were available to be compared with.

When a heavy projectile is ionized in a collision with a light target atom, this typically leads to a simultaneous ionization of the target atom. Fully differential measurements of these processes have been performed with reaction microscopes [67] at projectile kinematic energies from a few MeV/u [9–11,68] up to 1 GeV/u [69]. Since the target atom experiences a strong perturbation by the projectile ion in these collisions, the corresponding distribution of electrons ionized from the target can be described only by models beyond first-order perturbation theory [70–72]. Due to experimental restrictions the ionization of the target atom is not considered here.

Within this paper we present the measurement of the ELC for a few-electron heavy-ion projectile in the low-relativistic collision energy regime. For projectile ions of berylliumlike U^{88+} colliding with a nitrogen gas target at an energy of 90 MeV/u, the energy (or rather the momentum) distribution of electrons emitted at an angle of $\vartheta_e = 0^\circ$ with respect to the projectile beam was measured in coincidence with the up-charged U^{89+} ions. The studied electron energy range was $E_e = 38$–100 keV. The individual contribution of K-ELC originating from the projectile $1s$-shell ionization could be observed and distinguished from the dominating L-ELC originating from the $2s$-shell ionization. The measured spectra are compared to theoretical fully relativistic calculations using first-order perturbation theory.

The paper is organized as follows: Sec. II describes the experimental setup, Sec. III explains the data analysis, Sec. IV gives a short summary of the theory applied to the studied collision process, and Sec. V shows the experimental results in comparison with theory.

II. EXPERIMENT

The experiment was conducted at the heavy-ion accelerator facility GSI Helmholtzzentrum für Schwerionenforschung. The accelerator chain provided U^{73+} ions from the heavy-ion synchrotron SIS, which were stripped by a carbon foil with a thickness of 29 mg/cm^2 at about 90 MeV/u and charge analyzed. The choice of the collision energy was determined by the RECC experiment conducted simultaneously [8]. After injection of typically 10^8 ions of U^{88+} into the experimental storage ring ESR, electron cooling was applied. The resulting longitudinal momentum spread of the projectile-ion beam was $\Delta p_p/p_p \approx 10^{-4}$ at a well-defined ion beam energy of 90.38 MeV/u. After precooling, the ion beam was overlapped with a transverse supersonic gas-jet target of molecular nitrogen N_2 with a particle area density of about 10^{12} cm^{-2} [73]. This corresponded to an average luminosity on the order of $L \approx 100$ b^{-1} s^{-1}. Due to the excellent vacuum in the ESR of a few times 10^{-11} mbar, the beam lifetime of the circulating ion beam was mainly limited by charge-changing collisions within the gas-jet target. Because of the comparably large ionization and capture cross sections for U^{88+} at the present ion energy, an injection was repeated every 60 s.

The interaction zone was defined by the overlap between the horizontal U^{88+} projectile beam and the vertical nitrogen gas-jet target. As such, the length of the interaction zone was given by the target diameter of about 5 mm, and its transverse diameter was given by the size of the projectile beam of about 2 mm. Electrons ejected from the interaction zone into the forward direction parallel to the projectile beam were measured by a magnetic electron spectrometer (Fig. 1). The spectrometer consisted of two 60°-dipole magnets, each with a bending radius of 229 mm, and an iron-free quadrupole triplet between the dipole magnets. The first 60°-dipole magnet located 790 mm downstream from the interaction zone served both to magnetically separate the electrons from the ion beam and to filter a defined electron momentum range. Its magnetic field was measured by a Hall probe, whose values determined the electron momentum on a relative scale with a precision of better than 10^{-3}. The slight influence of the first spectrometer dipole magnet on the ion beam circulating in the storage ring was compensated by correction coils in the subsequent dipole magnet of the ring. The sequence of first spectrometer dipole, quadrupole triplet, and second dipole provided an achromatic optics. This optimized the momentum acceptance as well as the angular acceptance of the electrons, which were guided by the spectrometer from

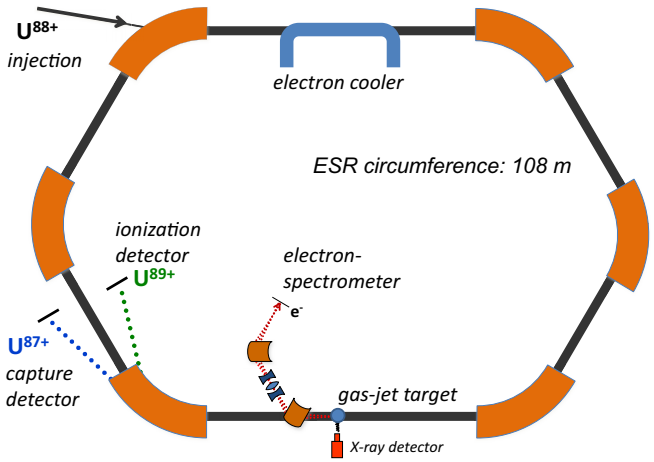

FIG. 1. (Color online) Layout of the experimental setup at the storage ring ESR with the electron cooler, the gas-jet target, the electron spectrometer and the particle detectors for projectile ionization and capture (from [8]).

the interaction point to a position-sensitive electron detector. To compensate the effect of the earth's magnetic field on the electron trajectory, two pairs of Helmholtz coils were mounted along the spectrometer. A combination of two microchannel plates (MCPs) in chevron configuration and a hexagonal delay-line anode was used as an electron detector. The hexagonal delay-line anode consisting of three independent wire pairs provided redundant reconstruction information of the electron impact position and assured a decreased dead time, compared to conventional rectangular delay-line anodes [74]. The information of the electron impact position ensured that the electrons guided through the spectrometer were always hitting the detector on a well-defined area. The traveling distance for the electrons from the interaction point to the electron detector was 4.2 m, the diameter of the aperture was everywhere along its path greater than 90 mm, and the diameter of the active area of the detector was 75 mm. On this active area, the electrons hit the detector within a spot of 30 mm diameter. The geometry and optics of the spectrometer permitted detection of electrons emitted from the gas-jet target within the whole azimuthal emission angle of $\varphi_e = 0^\circ$–360° for a polar angle $\vartheta_e = 0^\circ$–$\vartheta_{\max} = 0^\circ$–$2.4^\circ$ with respect to the beam axis, and a momentum spread of $\Delta p_e/p_e = 0.02$. These instrumental parameters were confirmed by electron optical calculations. The long distance between the interaction point and the electron detector additionally served well to suppress background from electrons scattered along the storage ring. However, time-of-flight effects were not considered since differences in the time of flight across the measured electron energy range could not be resolved experimentally.

As mentioned in the Introduction, electrons seen in the spectrometer for the collision system $U^{88+}(1s^2 2s^2) + N_2$ at 90 MeV/u originate from three competing processes with different underlying physical mechanisms. Besides the ELC discussed in this publication,

$$U^{88+} + N_2 \rightarrow U^{89+} + [N_2]^* + e^-, \tag{1}$$

the radiative electron capture to continuum [8]

$$U^{88+} + N_2 \rightarrow U^{88+} + [N_2^+]^* + e^- + \gamma \tag{2}$$

and the electron capture to continuum [33]

$$U^{88+} + N_2 \rightarrow U^{88+} + [N_2^+]^* + e^- \tag{3}$$

were measured and analyzed. Therefore, the double-differential cross sections for ELC were determined by counting electrons in coincidence with the up-charged U^{89+} projectiles, which were magnetically separated by the first dipole magnet of the ESR downstream from the gas-jet target and detected by a multiwire proportional counter (MWPC) [75]. A second MWPC of the same type was used to detect the down-charged U^{87+} ions for the purpose of normalization.

While ELC for this collision system dominantly implies L-shell ionization of the projectile, the contribution of K-shell ionization to the total ELC could be determined by studying the channel

$$\begin{aligned} U^{88+}(1s^2 2s^2) + N_2 &\rightarrow U^{89+}(1s2s^2) + [N_2]^* + e^- \\ &\rightarrow U^{89+}(1s^2 2l) + [N_2]^* + e^- + \gamma. \end{aligned} \tag{4}$$

In this channel, K-shell ionization of the projectile leads to an excited state, which decays promptly via x-ray emission. In the first step, we cannot experimentally exclude simultaneous ionization and excitation to a $1s2s2p$ state. In the second step, the decay of the $1s2s^2$ state may either occur directly via $M1$ transition into the $1s^2 2s$ state, via two-electron one-photon decay into a $1s^2 2p$ state [76], or via Auger decay.[1] The corresponding x-ray energies and branching ratios given in Ref. [77] were used in the analysis. In order to detect these x rays emitted from the interaction zone, a standard high-purity germanium detector was mounted at the gas-jet target at $\vartheta_\gamma = 90^\circ$ with respect to the projectile beam in the horizontal plane (cf. Fig. 1).

III. DATA ANALYSIS

In storage rings, the projectile velocity v_p of an electron-cooled ion beam is given by the velocity of the electrons in the electron cooler, as soon as an equilibrium of the cooling force and the projectile energy loss in the gas-jet target is reached [78]. Thus, for a given cooler voltage, the kinetic energy of the electrons in the cooler (corrected for space-charge effects) is the same as that for cusp electrons, when they travel at a velocity equal to the projectile velocity $v_e = v_p$ after interaction with the gas-jet target. This cusp electron energy is therefore termed $E_0 = 49.58$ keV. From this value, the specific projectile kinetic energy of 90.38 MeV/u was deduced, as well as the projectile velocity in units of the speed of light $\beta = 0.4112$, or in atomic units $v_p = 137.036 \times \beta = 56.33$ a.u., and the corresponding Lorentz

[1] In principle, this Auger electron of $E_e' = 63$ keV [77] is also observable in the spectrometer at $E_e = 236$ keV. However, its signature is identical to that of L-ELC, i.e., the up-charged projectile U^{89+} in coincidence with the electron, and its cross section in the laboratory frame is orders of magnitude lower.

factor $\gamma = 1 + E_0/(m_e c^2) = 1.097$. These values are used throughout this paper.

The energy axis of the measured electron distribution was determined as follows: The magnetic field of the first momentum-analyzing dipole of the spectrometer was measured on a relative scale using a Hall probe with a precision on the level of 10^{-3}. After transforming the relative momentum scale to a relative kinetic energy scale the electron spectrum was calibrated in the maximum of the ELC distribution to the cusp energy E_0, assuming that the distribution is quasisymmetric around E_0, as will be discussed in Sec. V. The accuracy of this calibration was estimated to be $\delta E_e/E_e = 0.01$. Since the same value for E_0 is used in both experiment and theory, the comparison of the two spectral shapes does not dependent on the precision to which E_0 is determined from the projectile-ion velocity.

For ELC from $U^{88+}(1s^2 2s^2)$—the sum of L-ELC and K-ELC—double-differential cross sections $d^2\sigma/dE_e d\Omega_e$ at $\vartheta_e = 0^\circ$ as a function of the electron kinetic energy E_e were determined from the number of electrons coincident with an up-charged projectile $N_{e\wedge\mathrm{loss}}$ as a function of the magnetic fields applied to the spectrometer. In the maximum of the cusp, the singles rate of the MCP was $\dot{N}_e \approx 250$ Hz and the true coincidence rate $\dot{N}_{e\wedge\mathrm{loss}} \approx 75$ Hz, while the MWPC rate of ionized projectiles was $\dot{N}_{\mathrm{loss}} \approx 250$ kHz. Due to the excellent time resolution of the MCP for the electrons and the MWPC for up-charged projectiles, the coincidence spectrum showing the time difference between a MCP signal and a MWPC signal had a sharp peak with a width of 10 ns and with a ratio of true-to-random coincidences of better than 25:1.

From $N_{e\wedge\mathrm{loss}}$ the cross sections were calculated through

$$\left.\frac{d^2\sigma^{\mathrm{ELC}}}{dE_e d\Omega_e}\right|_{\vartheta_e=0^\circ} = \frac{N_{e\wedge\mathrm{loss}}}{L_{\mathrm{int}}}\frac{1}{\epsilon_e \Delta\Omega_e}\frac{E_e + m_e c^2}{E_e^2 + 2E_e m_e c^2}\frac{1}{\Delta p_e/p_e} \tag{5}$$

with the electron detection efficiency ϵ_e, the observation solid angle $\Delta\Omega_e \approx \pi\vartheta_{\mathrm{max}}^2$, and the relative momentum acceptance $\Delta p_e/p_e$ of the spectrometer. The MWPC detecting the up-charged projectiles had an efficiency close to 100% [75]. The energy factor with the electron rest energy $m_e c^2$ includes both the transformation of momentum-differential to energy-differential cross sections dp_e/dE_e and the dispersion correction $1/p_e(\Delta p_e/p_e)$, i.e., the increasing absolute momentum acceptance with increasing momentum. The integrated luminosity L_{int} in units of b^{-1} was determined by integration of the product of ion beam current $I_{\mathrm{ion}}(t)$ and target area density $n_{\mathrm{target}}(t)$ over the measurement time t,

$$L_{\mathrm{int}} = \int \frac{I_{\mathrm{ion}}(t) n_{\mathrm{target}}(t)}{Z_p e} dt \tag{6}$$

with $Z_p e = 88e$ being the projectile charge.

Double-differential cross sections for the contribution of K-ELC were determined from the number of electrons coincident with the up-charged projectile and the corresponding x ray $N_{e\wedge\mathrm{loss}\wedge\gamma}$. Additionally, background was suppressed by taking only those events into account where the energy of the emitted photon $E_\gamma = E'_\gamma/\gamma$ was in the correct range, with the projectile frame energy from the deexcitation of the $1s2s^2$ state being $E'_\gamma \approx 95$ keV [77]. These four conditions provided a clean identification of K-ELC events. The spectrum was calculated by

$$\left.\frac{d^2\sigma^{K\text{-ELC}}}{dE_e d\Omega_e}\right|_{\vartheta_e=0^\circ} = \frac{N_{e\wedge\mathrm{loss}\wedge\gamma}}{L_{\mathrm{int}}}\frac{1}{\epsilon_e \Delta\Omega_e}\frac{4\pi}{\epsilon_\gamma \Delta\Omega_\gamma}\frac{\gamma^2}{a_\gamma}\frac{E_e + m_e c^2}{E_e^2 + 2E_e m_e c^2}\frac{1}{\Delta p_e/p_e}. \tag{7}$$

Here, ϵ_γ is the photon detection efficiency and $\Delta\Omega_\gamma \approx 10^{-3}\times 4\pi$ the observation solid angle of the x-ray detector mounted at $\vartheta_\gamma = 90^\circ$. The photon originating from the decay of the $U^{89+}(1s2s^2)$ state is emitted isotropically in the projectile frame [77]. The solid-angle transformation of the photon distribution into the laboratory frame introduces a factor $d\Omega_\gamma/d\Omega'_\gamma = \gamma^2(1 - \beta\cos\vartheta_\gamma)^2 = \gamma^2$. Furthermore, the theoretical branching ratio of radiative decay $a_\gamma = 73.8\%$ versus Auger decay was taken from [77].

A relative systematic error of the experimental data of 15% was estimated from uncertainties in the reproducibility and the energy dependence of the spectrometer efficiency while scanning its magnetic fields. In order to avoid uncertainties in the determination of L_{int} through Eq. (6), an independent normalization to the recombined U^{89+} ions detected in the corresponding MWPC was used. The statistical error for the ELC measurement was around 0.2% and thus negligible, but the statistical error for the K-ELC was about 20%–40% due to its smaller cross section and the small x-ray detection angle $\Delta\Omega_\gamma$.

Absolute cross sections were not derived from the data due to the unknown detection efficiencies for the electrons ϵ_e and the photons ϵ_γ, and uncertainties in the branching ratio a_γ. The relative cross sections resulting from Eqs. (5) and (7) were therefore normalized to theory by multiplication with a constant factor, which was determined as the weighted average of the ratio of experimental data and theory. The corresponding residuals are shown at the bottom of Figs. 4 and 5.

IV. THEORY

In the present investigation we explore the projectile-electron loss in very asymmetric collisions, in which the charge of the projectile nucleus (and the net charge of the projectile Z_p) greatly exceeds that of the target nucleus. In spite of the seemingly very high impact energy, the collision velocity $v_p = 56.33$ a.u. is very large only on the velocity scale of the bound target electrons ($v_t^b \approx Z_t$), whereas it is close to the classical orbiting velocities of the $2s$ electrons of the ion and by about a factor of 2 lower than those of the K-shell electrons. For comparison, the projectile velocity corresponds to an electron kinetic energy of $E_0 = 49.58$ keV (cf. Sec. II), the binding energy of a $2s$ electron in $U^{88+}(1s^2 2s^2)$ amounts to $E_p^b(2s) = 32.37$ keV [79], and the ionization of the $1s$ electron into a $U^{89+}(1s2s^2)$ configuration requires $E_p^b(1s) = 128.3$ keV [77,79].

In the target frame the minimum momentum transfer in the collision is given by

$$q_{\min} = \frac{E_t^f - E_t^i}{v_p} + \frac{E_p^f - E_p^i}{\gamma v_p} \tag{8}$$

$$= \frac{E_t^f + |E_t^b|}{v_p} + \frac{E_e' + |E_p^b|}{\gamma v_p}. \tag{9}$$

Here, E_t^i, E_t^f, E_p^i, and E_p^f are, respectively, the initial and the final energy of the target and the projectile electron. They are equivalent to the electron binding energies E_t^b and E_p^b, and the projectile-frame kinetic energy of the observed electron E_e'. The final energy of the target electron E_t^f, which is for nitrogen typically a few eV, is not observed in this experiment.

It follows from Eq. (8), that the collisions resulting in the loss of a very tightly bound (K-shell) electron from the ion are characterized by momentum transfers $q \approx Z_p^2/2\gamma v_p \gg 1$, which are very large on the scale of the target atom. Under such conditions one may regard the target atom as incoherent superposition of the atomic nucleus and the atomic electrons, which behave in the collision as (quasi)free particles with respect to each other, and it is the field of the projectile nucleus which determines not only the motion of the electrons of the projectile but also the motion of the atomic target [80]. The required large momentum transfer can be provided only at small impact parameters $b \approx 1/q$, which are well inside the classical K-shell orbit of the target atom, such that the atomic nucleus can be treated as an unscreened Coulomb potential.

The charge of the atomic nucleus Z_t is much smaller than that of the highly charged projectile Z_p. Therefore, compared to the field of the ion, the field of the atomic nucleus represents merely a weak perturbation for the active electron of the ion, and its action may be described within the first-order perturbation theory in the interaction between this electron and the atomic nucleus. Since the atomic nucleus has a very large mass, the distortion of its motion by the field of the ion can be ignored, and its initial and final states can be approximated by plane waves.

Similarly, the field of the atomic electrons is also just a weak perturbation for the electron of the ion, and its action on the latter can be described in the first-order approximation in the electron-electron interaction. However, in contrast to the atomic nucleus the electrons of the atom cannot be approximated by plane waves since the field of the projectile substantially distorts their motion. This distortion may have an important effect on the interaction of these electrons with the active electron of the ion [81].

In our present calculations the interaction between the electrons of the projectile and the nucleus of the target was described within the first order of perturbation theory by applying one-electron Dirac wave functions. For the L-shell ionization of the projectile the screening by its K-shell electrons was considered by applying a Coulomb potential with an effective nuclear charge of $Z_{\text{eff}} = 90$. The nucleus of the projectile was regarded as infinitely heavy, and the motion of the nucleus of the atom was approximated by plane waves. Details of the calculation are given in [12,15,17]. Due to the high momentum transfers considered here, the molecular character of the N_2 target was ignored, and all cross sections are given per target atom N.

The theoretical double-differential cross sections $d^2\sigma/dE_e'd\Omega_e'$ were calculated in the (primed) projectile frame. Exemplary angular distributions of the emitted

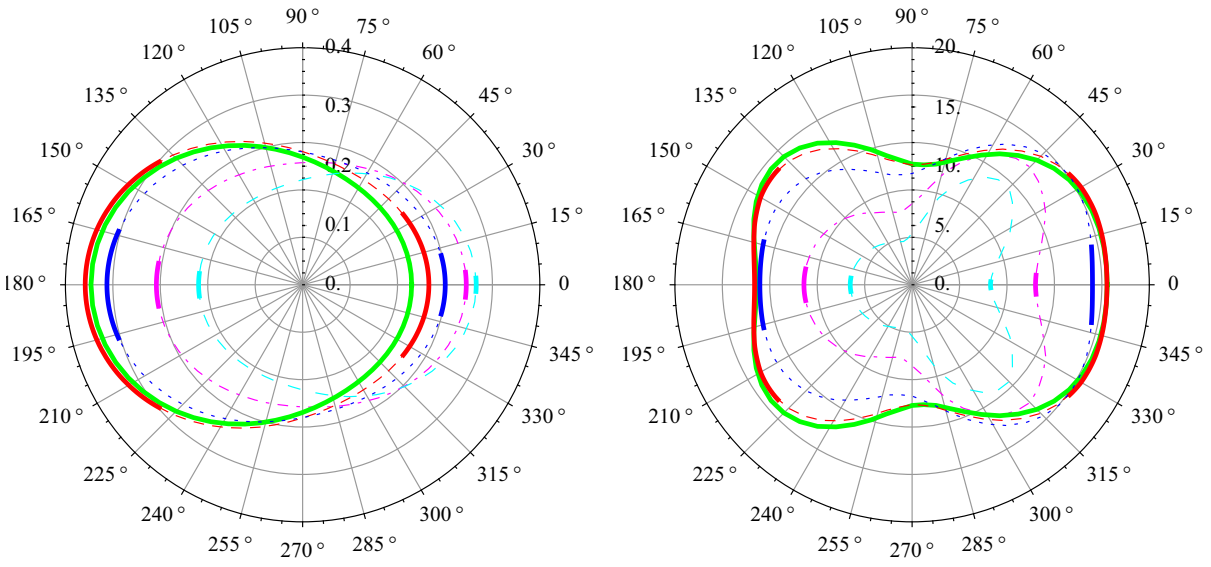

(a) K-ELC (b) L-ELC

FIG. 2. (Color online) Electron loss to continuum (ELC) in collisions (a) $U^{88+}(1s^22s^2) + N \rightarrow U^{89+}(1s2s^2) + N^* + e^-(E_e', \vartheta_e')$ and (b) $U^{88+}(1s^22s^2) + N \rightarrow U^{89+}(1s^22s) + N^* + e^-(E_e', \vartheta_e')$ at a collision energy of 90 MeV/u. The theoretical double-differential cross sections $d^2\sigma/dE_e'd\Omega_e'$ in b/(keV sr) are shown as a function of the polar emission angle of the electron, ϑ_e', in the projectile frame for various emission energies of the electron: $E_e' = 0.047$ keV (solid green line), $E_e' = 0.192$ keV (short-dashed red line), $E_e' = 1.094$ keV (dotted blue line), $E_e' = 5.054$ keV (dot-dashed magenta line), and $E_e' = 11.542$ keV (long-dashed cyan line). The intervals of the angular distributions marked in bold fall into the angular acceptance of the electron spectrometer in the laboratory system.

electron as a function of the polar scattering angle ϑ_e for the collision system studied here are shown in Figs. 2(a) and 2(b) for the K-ELC and L-ELC, respectively. In order to compare these to the experimental data, they were transformed into the (unprimed) laboratory frame and averaged over the polar angular acceptance of the spectrometer, $0^\circ \leqslant \vartheta_e \leqslant \vartheta_{\max}$, with $\vartheta_{\max} = 2.4^\circ$. Since the electron angular distribution is independent of the azimuthal emission angle φ'_e and the Lorentz transformation implies $d\varphi'_e = d\varphi_e$, the electron energy distribution measured in the laboratory was given by

$$\left.\frac{d^2\sigma}{dE_e d\Omega_e}\right|_{\vartheta_e=0^\circ} = \frac{1}{1-\cos\vartheta_{\max}} \int_0^{\vartheta_{\max}} \frac{d^2\sigma}{dE'_e d\Omega'_e} \sin\vartheta'_e d\vartheta_e. \tag{10}$$

Furthermore, the momentum acceptance of the spectrometer $\Delta p_e/p_e = 0.02$ was taken into account by convolving the results of Eq. (10) with the corresponding energy acceptance $\Delta E_e/E_e = (\gamma+1)/\gamma \times \Delta p_e/p_e \approx 2\times\Delta p_e/p_e$.

We note that the projectile frame is rotated by 180° with respect to the laboratory frame, such that the projectile-frame angle ϑ'_e is related to the corresponding angle ϑ_e by means of

$$\vartheta'_e(E_e,\vartheta_e) = \pi - \arctan\left[\frac{\sin\vartheta_e}{\gamma[\cos\vartheta_e - \beta/\beta_e(E_e)]}\right] \tag{11}$$

with the projectile velocity β and the velocity of the emitted electron $\beta_e(E_e)$. The dependencies $\vartheta'_e(E_e,\vartheta_e)$ and $E'_e(E_e,\vartheta_e)$ lead to the fact that a two-dimensional interpolation of grid points of the double-differential cross section in the projectile frame is needed in order to evaluate the double-differential cross section in the laboratory frame through Eq. (10).

In Fig. 2 the emission angles ϑ'_e with $0^\circ \leqslant \vartheta'_e \leqslant \vartheta'_{\max} \leqslant 90^\circ$ for $E_e < E_0$ and $180^\circ \geqslant \vartheta'_e \geqslant \vartheta'_{\max} \geqslant 90^\circ$ for $E_e > E_0$ that fall into the angular acceptance of the spectrometer $\vartheta_{\max} = 2.4^\circ$ are marked in bold. For comparison Fig. 3 shows the single-differential cross sections in the projectile frame $d\sigma/dE'_e$ as a function of the energy of the emitted electron E'_e, integrated over all electron emission angles. The spectra reveal

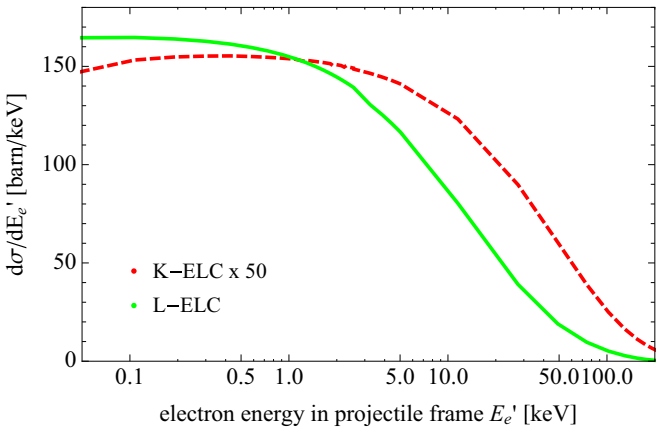

FIG. 3. (Color online) Single-differential cross section $d\sigma/dE'_e$ of K-ELC (dashed red line) and L-ELC (solid green line) in the projectile frame as a function of the energy of the emitted electron for the collision system U^{88+} + N at a collision energy of 90 MeV/u. For better comparison of the spectral shape the K-ELC cross section is multiplied by 50.

an approximately constant single-differential cross section in the projectile frame $d\sigma/dE'_e$ for small continuum electron energies $E'_e < 1$ keV. The strong peak structure of the ELC observed in the laboratory frame around $E_e \approx E_0$ is thus generated only by the fact that a larger fraction of the angular distribution will contribute to the energy distribution in the laboratory for small energies E'_e.

V. RESULTS AND DISCUSSION

Figure 4 shows the experimental results of the double-differential cross section $d^2\sigma/dE_e d\Omega_e$ for electrons emitted under $\vartheta_e = 0^\circ$–2.4° as a function of the kinetic energy E_e of the emitted electron in comparison with theory. A good agreement is achieved. The theoretical curves illustrate that the ELC spectrum is dominated by projectile ionization of the L shell, whereas the contribution of ionization of the K shell is on the 2% level. This behavior is evident when we compare the corresponding electron binding energies given in Sec. IV: In an intuitive picture the collision energy is above the effective L-shell ionization threshold, but below the K-shell ionization threshold for electron impact ionization. Nevertheless K-shell ionization is possible in the Coulomb field of the N-target nucleus, as can be seen in Fig. 5. Clearly the experimental data deduced via Eq. (7) are dominated by statistical uncertainties due to the small cross section and the small photon observation angle $\Delta\Omega_\gamma \approx 10^{-3}\times 4\pi$. Consequently the experimental results do not provide a

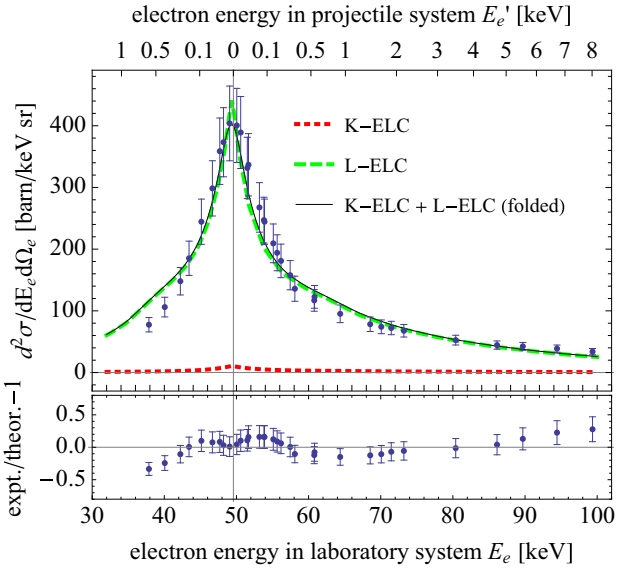

FIG. 4. (Color online) Top: Double-differential cross section for the electron loss to continuum observed at $\vartheta_e = 0^\circ$ for collisions of $U^{88+}(1s^2 2s^2)$ + N at 90 MeV/u. Displayed are the experimental data (symbols), the theory for K-ELC (dotted red line), the theory for L-ELC (dashed green line), and the sum of theoretical results for K-ELC and L-ELC folded with the spectrometer resolution (solid black line). The theoretical calculations imply that the cross section is dominated by electrons from the L shell of the projectile, while the projectile K-shell electrons contribute about 2% to the total cross section (cf. Fig. 5). Bottom: Relative residuals of the experimental results scaled to theory.

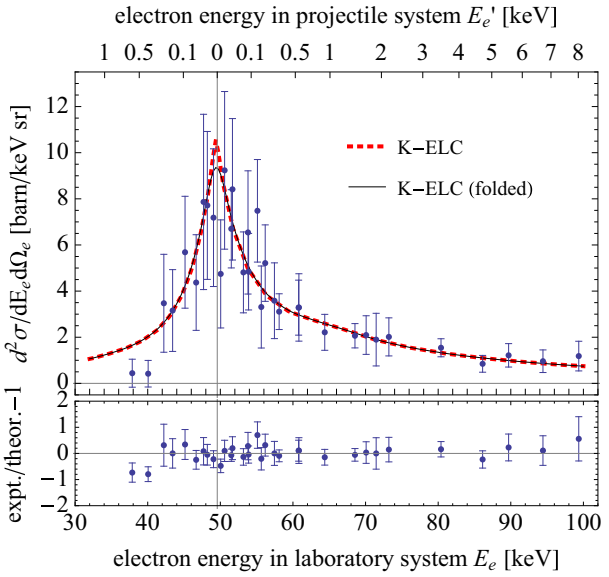

FIG. 5. (Color online) Top: Contribution of projectile K-shell electrons to the electron loss to the continuum shown in Fig. 4. Displayed are the experimental data (symbols), the theory for K-ELC (dotted red line), and the theory for K-ELC folded with spectrometer resolution (solid black line). Bottom: Relative residuals of the experimental results scaled to theory.

stringent test for theory, but still the parallel existence of both channels is confirmed by the data.

The electron cusp of the L-ELC given in Fig. 4 does not show a significant asymmetry. In contrast the electron distribution in the projectile frame depicted in Fig. 2 shows a clear forward-to-backward asymmetry. This, however, is compensated in the Lorentz transformation by the variation of the angular acceptance in the projectile frame $\vartheta'_{\max}(E_e, \vartheta_{\max})$ through Eq. (11). As seen in Fig. 2 by the intervals of the angular distribution marked in bold, the angular acceptance is larger for electrons emitted around $\vartheta'_e = 180^\circ$ compared to electrons emitted around $\vartheta'_e = 0^\circ$, i.e.,

$$\vartheta'_{\max}(E_e < E_0, \vartheta_{\max}) \; < \; |180^\circ - \vartheta'_{\max}(E_e > E_0, \vartheta_{\max})|.$$

Keeping in mind that the projectile frame is rotated by 180° with respect to the laboratory frame it becomes clear that the electron distribution of the K-ELC shown in Fig. 2 leads to a small asymmetry in the (theoretical) spectra of Fig. 5 with a preference towards the high-energy side of the cusp.

The influence of the angular acceptance of the spectrometer $\vartheta_{\max}$ on the cusp shape was studied by evaluation of the theoretical double-differential cross section of Eq. (10) for different values of $\vartheta_{\max}$ around 2.4°. Since in this formula the cross sections are normalized to the angular acceptance, they are comparably large on the absolute scale. In the wings of the distribution the cross section does not change noticeably when varying $\vartheta_{\max}$, because the angular distribution in the projectile frame is approximately constant within the integration angle $\vartheta'_{\max}$ at these electron energies. For example, the deviation of the cross section for $\vartheta_{\max} = 2.0^\circ$ instead of 2.4° is less than 5% for $|E_e - E_0| > 4$ keV. In contrast, the cusp shape at its maximum $E_e \approx E_0$, where $\vartheta'_{\max} \approx 90^\circ$, is clearly influenced by the value of $\vartheta_{\max}$. The cross section around E_0 increases with decreasing $\vartheta_{\max}$, and vice versa. In the limiting case $\vartheta_{\max} \to 0$, the prefactor of Eq. (10) $1/(1 - \cos\vartheta_{\max}) \approx 2/\vartheta^2_{\max}$ leads to a divergence of the cross section at $E_e = E_0$, as is well known from electron cusp physics [27,39]. As a side note it should be mentioned that the finite energy resolution of the spectrometer also lowers the maximum of the cusp shape while having no effects on the wings of the cusp, as shown in Figs. 4 and 5.

In the analysis the measured relative cross sections are normalized to the theoretical calculations, which account for only the atomic target nucleus and neglect the influence of the atomic target electrons. The appropriateness of this approach can be estimated by the following considerations. In the case of the electron loss from the K shell of the projectile it is fully justified to neglect the atomic electrons, since the collision velocity is substantially higher than the effective threshold velocity for the loss by the impact of a free electron. In case of the loss from the L shell, where the collision velocity is larger than the corresponding threshold velocity, one would normally argue that one can still ignore the effect of the atomic electrons, since the contributions to the loss from the interactions with the nucleus and electrons of the atom scale as $\sim Z_t^2$ and $\sim Z_t$, respectively, and thus the electrons of nitrogen would yield just about 14% of the loss cross section. However, according to the results of [81], one may expect that in the range of impact velocities not very far from the effective threshold the electrons are more effective in producing ionization than equal-velocity protons. Therefore, the uncertainty in the calculated results for the loss from the L shell, which is introduced by neglecting the atomic electrons, could be noticeably larger than $1/Z_t \approx 14\%$. In addition, these two channels of electron loss could also lead to different angular and energy distributions of the emitted electrons that can make the effect of the atomic electrons even more visible. But, as can be seen when comparing Figs. 2(a) and 2(b) with Figs. 4 and 5, the details of the electron distribution in the projectile frame are partially smeared out by the transformation into the laboratory frame. Therefore, it is expected that neglecting the effect of the atomic electrons does not lead to a substantial change in the spectral shape, but rather to a slight increase in the absolute scale of the cross sections.

Experimental uncertainties might arise from a small fraction of U^{88+} ions in the metastable $^3P_0$ state, possibly produced in the carbon stripper foil just before injection into ESR. According to [82] these ions might not fully decay into the $^1S_0$ ground state during the beam preparation time of about 8 s, before the measurement phase begins. However, their fraction averaged over the measurement time of 48 s is negligible. Moreover, the excitation energy of 258 eV [83] indicates that the electron distribution for electrons ionized from the $^3P_0$ state should not vary significantly from that of the $^1S_0$ state.

VI. SUMMARY AND OUTLOOK

Relative cross sections for electron loss to the continuum as a function of the electron energy have been measured for highly charged U^{88+} ions colliding with a nitrogen-gas target. The low-relativistic collision energy of 90 MeV/u was chosen such that the projectile velocity is comparable to the

effective threshold velocity for ionization of the uranium L shell by electron impact. The experimental results were successfully described by theoretical calculations using Dirac wave functions, where the interaction between the electron of the projectile and the nucleus of the target is treated in first-order perturbation theory. By comparing the theoretical results in the projectile and the laboratory frames, it was demonstrated that the quasisymmetric electron cusp of the L-ELC in the laboratory frame results from a compensation of the asymmetric electron distribution in the projectile frame by the Lorentz transformation from the projectile to the laboratory frame. The K-ELC could be observed by applying a triple coincidence between the up-charged projectile, the electron, and the emitted photon from the subsequent deexcitation, but large statistical errors prevented a stringent test of theory for this spectrum.

Obviously, a next desirable step is to measure the ELC using a U^{91+} projectile to unambiguously identify the shape of the K-ELC. With an increased experimental accuracy the difference in the line shapes of K- and L-ELC can be investigated. Deepening the understanding of the electron loss to the continuum certainly includes the study of the contribution to the projectile ionization by the electrons of the target atom in comparison to the ionization by the nucleus of the target atom. Similar experiments performed for projectile excitation in collisions of heavy ions with light atoms [6] can be extended to the field of projectile ionization by very light target atoms such as hydrogen at projectile energies near the effective ionization threshold, where the nucleus and the electrons of the target atom may have significantly varying contributions to the electron cusp [80,81]. Also, the application of heavier target atoms with an atomic number $Z_t \approx v_p$ such as xenon would provide tests for theoretical models beyond first-order perturbation theory [14].

ACKNOWLEDGMENTS

P.-M.H. gratefully acknowledges the support by HIC-for-FAIR through HGS-HIRe. This work was supported by the Helmholtz-CAS Joint Research Group HCJRG-108, by the Helmholtz Alliance Program of the Helmholtz Association Contract No. HA216/EMMI (Extremes of Density and Temperature: Cosmic Matter in the Laboratory), by BMBF Contracts No. 06GI911I and No. 05P12R6FAN, and by the European Community FP7-Capacities Contract ENSAR No. 262010.

[1] J. Eichler and T. Stöhlker, Phys. Rep. **439**, 1 (2007).
[2] Y. A. Litvinov and F. Bosch, Rep. Prog. Phys. **74**, 016301 (2011).
[3] T. Stöhlker, T. Ludziejewski, H. Reich, F. Bosch, R. W. Dunford, J. Eichler, B. Franzke, C. Kozhuharov, G. Menzel, P. H. Mokler, F. Nolden, P. Rymuza, Z. Stachura, M. Steck, P. Swiat, A. Warczak, and T. Winkler, Phys. Rev. A **58**, 2043 (1998).
[4] T. Stöhlker, T. Ludziejewski, F. Bosch, R. W. Dunford, C. Kozhuharov, P. H. Mokler, H. F. Beyer, O. Brinzanescu, B. Franzke, J. Eichler, A. Griegal, S. Hagmann, A. Ichihara, A. Krämer, J. Lekki, D. Liesen, F. Nolden, H. Reich, P. Rymuza, Z. Stachura, M. Steck, P. Swiat, and A. Warczak, Phys. Rev. Lett. **82**, 3232 (1999).
[5] S. Trotsenko, A. Kumar, A. V. Volotka, D. Banaś, H. F. Beyer, H. Bräuning, S. Fritzsche, A. Gumberidze, S. Hagmann, S. Hess, P. Jagodziński, C. Kozhuharov, R. Reuschl, S. Salem, A. Simon, U. Spillmann, M. Trassinelli, L. C. Tribedi, G. Weber, D. Winters, and T. Stöhlker, Phys. Rev. Lett. **104**, 033001 (2010).
[6] A. Gumberidze, D. B. Thorn, C. J. Fontes, B. Najjari, H. L. Zhang, A. Surzhykov, A. Voitkiv, S. Fritzsche, D. Banaś, H. Beyer, W. Chen, R. D. DuBois, S. Geyer, R. E. Grisenti, S. Hagmann, M. Hegewald, S. Hess, C. Kozhuharov, R. Märtin, I. Orban, N. Petridis, R. Reuschl, A. Simon, U. Spillmann, M. Trassinelli, S. Trotsenko, G. Weber, D. F. A. Winters, N. Winters, D. Yu, and T. Stöhlker, Phys. Rev. Lett. **110**, 213201 (2013).
[7] M. Nofal, S. Hagmann, T. Stöhlker, D. H. Jakubassa-Amundsen, C. Kozhuharov, X. Wang, A. Gumberidze, U. Spillmann, R. Reuschl, S. Hess, S. Trotsenko, D. Banas, F. Bosch, D. Liesen, R. Moshammer, J. Ullrich, R. Dörner, M. Steck, F. Nolden, P. Beller, H. Rothard, K. Beckert, and B. Franczak, Phys. Rev. Lett. **99**, 163201 (2007).
[8] P.-M. Hillenbrand, S. Hagmann, D. Atanasov, D. Banaś, K.-H. Blumenhagen, C. Brandau, W. Chen, E. De Filippo, A. Gumberidze, D. L. Guo, D. H. Jakubassa-Amundsen, O. Kovtun, C. Kozhuharov, M. Lestinsky, Y. A. Litvinov, A. Müller, R. A. Müller, H. Rothard, S. Schippers, M. S. Schöffler, U. Spillmann, A. Surzhykov, S. Trotsenko, N. Winckler, X. L. Yan, V. A. Yerokhin, X. L. Zhu, and T. Stöhlker, Phys. Rev. A **90**, 022707 (2014).
[9] D. Fischer, M. Schulz, K. Schneider, M. F. Ciappina, T. Kirchner, A. Kelkar, S. Hagman, M. Grieser, K.-U. Kühnel, R. Moshammer, and J. Ullrich, Phys. Rev. A **80**, 062703 (2009).
[10] X. Wang, K. Schneider, A. Kelkar, M. Schulz, B. Najjari, A. Voitkiv, M. Gundmundsson, M. Grieser, C. Krantz, M. Lestinsky, A. Wolf, S. Hagmann, R. Moshammer, J. Ullrich, and D. Fischer, Phys. Rev. A **84**, 022707 (2011).
[11] D. Fischer, D. Globig, J. Goullon, M. Grieser, R. Hubele, V. L. B. de Jesus, A. Kelkar, A. LaForge, H. Lindenblatt, D. Misra, B. Najjari, K. Schneider, M. Schulz, M. Sell, and X. Wang, Phys. Rev. Lett. **109**, 113202 (2012).
[12] A. Voitkiv, Phys. Rep. **392**, 191 (2004).
[13] A. B. Voitkiv, B. Najjari, and J. Ullrich, Phys. Rev. A **75**, 062716 (2007).
[14] A. B. Voitkiv, B. Najjari, and J. Ullrich, Phys. Rev. A **76**, 022709 (2007).
[15] A. Voitkiv and J. Ullrich, *Relativistic Collisions of Structured Atomic Particles*, Springer Series on Atomic, Optical, and Plasma Physics No. 49 (Springer, Berlin, 2008).
[16] A. B. Voitkiv, J. Phys. B **40**, 2885 (2007).
[17] A. Surzhykov and S. Fritzsche, J. Phys. B **38**, 2711 (2005).
[18] T. Stöhlker, D. C. Ionescu, P. Rymuza, F. Bosch, H. Geissel, C. Kozhuharov, T. Ludziewjewski, P. H. Mokler, C. Scheidenberger, Z. Stachura, A. Warczak, and R. W. Dunford, Phys. Rev. A **57**, 845 (1998).
[19] A. Gumberidze, S. Fritzsche, F. Bosch, D. C. Ionescu, A. Krämer, C. Kozhuharov, Z. Stachura, A. Surzhykov, A. Warczak, and T. Stöhlker, Phys. Rev. A **82**, 052712 (2010).

[20] A. Gumberidze, S. Fritzsche, S. Hagmann, C. Kozhuharov, X. Ma, M. Steck, A. Surzhykov, A. Warczak, and T. Stöhlker, Phys. Rev. A **84**, 042710 (2011).

[21] M. Breinig, S. B. Elston, S. Huldt, L. Liljeby, C. R. Vane, S. D. Berry, G. A. Glass, M. Schauer, I. A. Sellin, G. D. Alton, S. Datz, S. Overbury, R. Laubert, and M. Suter, Phys. Rev. A **25**, 3015 (1982).

[22] K. O. Groeneveld, W. Meckbach, and I. A. Sellin, *Forward Electron Ejection in Ion Collisions*, Lecture Notes in Physics Vol. 213 (Springer, Berlin, 1984).

[23] N. Stolterfoht, *Electron Emission in Heavy Ion-Atom Collisions*, Springer Series on Atomic, Optical, and Plasma Physics No. 20 (Springer, Berlin, 1997).

[24] M. E. Rudd, C. A. Sautter, and C. L. Bailey, Phys. Rev. **151**, 20 (1966).

[25] J. Macek, Phys. Rev. A **1**, 235 (1970).

[26] G. Crooks and M. Rudd, Phys. Rev. Lett. **25**, 1599 (1970).

[27] K. Dettmann, K. G. Harrison, and M. W. Lucas, J. Phys. B **7**, 269 (1974).

[28] C. R. Vane, I. A. Sellin, M. Suter, G. D. Alton, S. B. Elston, P. M. Griffin, and R. S. Thoe, Phys. Rev. Lett. **40**, 1020 (1978).

[29] J. Macek, J. E. Potter, M. M. Duncan, M. G. Menendez, M. W. Lucas, and W. Steckelmacher, Phys. Rev. Lett. **46**, 1571 (1981).

[30] J. Burgdörfer, Phys. Rev. A **33**, 1578 (1986).

[31] H. Knudsen, L. H. Andersen, and K. E. Jensen, J. Phys. B **19**, 3341 (1986).

[32] A. Skutlartz, S. Hagmann, and H. Schmidt-Böcking, J. Phys. B **21**, 3609 (1988).

[33] P.-M. Hillenbrand *et al.* (unpublished).

[34] S. Datz, R. Hippler, L. H. Andersen, P. F. Dittner, H. Knudsen, H. F. Krause, P. D. Miller, P. L. Pepmiller, T. Rosseel, R. Schuch, N. Stolterfoht, Y. Yamazaki, and C. R. Vane, Phys. Rev. A **41**, 3559 (1990).

[35] C. F. Chou, R. Koch, Y. C. Chang, C. C. Hsu, C. Kelbch, and H. Schmidt-Bocking, J. Phys. B **25**, 3505 (1992).

[36] D. H. Jakubassa-Amundsen, J. Phys. B **36**, 1971 (2003).

[37] D. H. Jakubassa-Amundsen, Eur. Phys. J. D **41**, 267 (2007).

[38] N. Stolterfoht, D. Schneider, D. Burch, H. Wieman, and J. Risley, Phys. Rev. Lett. **33**, 59 (1974).

[39] J. S. Briggs and F. Drepper, J. Phys. B **11**, 4033 (1978).

[40] J. S. Briggs and M. H. Day, J. Phys. B **13**, 4797 (1980).

[41] D. H. Jakubassa-Amundsen, J. Phys. B **14**, 3139 (1981).

[42] J. Burgdörfer, M. Breinig, S. B. Elston, and I. A. Sellin, Phys. Rev. A **28**, 3277 (1983).

[43] S. B. Elston, S. D. Berry, J. Burgdörfer, I. A. Sellin, M. Breinig, R. DeSerio, C. E. Gonzalez-Lepera, L. Liljeby, K. O. Groeneveld, D. Hofmann, P. Koschar, and I. B. E. Nemirovsky, Phys. Rev. Lett. **55**, 2281 (1985).

[44] K. F. Man, W. Steckelmacher, and M. W. Lucas, J. Phys. B **19**, 401 (1986).

[45] L. Sarkadi and A. Orbán, Phys. Rev. Lett. **100**, 133201 (2008).

[46] R. D. DuBois and S. T. Manson, Phys. Rev. Lett. **57**, 1130 (1986).

[47] O. Heil, J. Kemmler, K. Kroneberger, A. Kövér, G. Szabó, L. Gulyás, R. DeSerio, S. Lencinas, N. Keller, D. Hofmann, H. Rothard, D. Berényi, and K. O. Groeneveld, Z. Phys. D **9**, 229 (1988).

[48] A. Kover, L. Sarkadi, J. Palinkas, D. Berenyi, G. Szabo, T. Vajnai, O. Heil, K. O. Groeneveld, J. Gibbons, and I. A. Sellin, J. Phys. B **22**, 1595 (1989).

[49] O. Heil, R. D. DuBois, R. Maier, M. Kuzel, and K.-O. Groeneveld, Z. Phys. D **21**, 235 (1991).

[50] P. Závodszky, L. Sarkadi, J. Tanis, D. Berényi, J. Pálinkás, V. Plano, L. Gulyás, E. Takács, and L. Töth, Nucl. Instrum. Methods Phys. Res. B **79**, 67 (1993).

[51] H. Trabold, G. M. Sigaud, D. H. Jakubassa-Amundsen, M. Kuzel, O. Heil, and K. O. Groeneveld, Phys. Rev. A **46**, 1270 (1992).

[52] L. H. Andersen, M. Frost, P. Hvelplund, H. Knudsen, and S. Datz, Phys. Rev. Lett. **52**, 518 (1984).

[53] L. H. Andersen, M. Frost, P. Hvelplund, and H. Knudsen, J. Phys. B **17**, 4701 (1984).

[54] C. Liao, S. Hagmann, T. Zouros, E. Montenegro, G. Toth, P. Richard, S. Grabbe, and C. Bhalla, Nucl. Instrum. Methods Phys. Res. B **98**, 324 (1995).

[55] C. R. Vane, in *The Physics of Electronic and Atomic Collisions:XXI International Conference*, edited by Y. Itikawa, K. Okuno, H. Tanaka, A. Yagishita, and Michio Matsuzawa, AIP Conf. Proc. No. 500 (AIP, Melville, NY, 2000), pp. 709–714.

[56] A. B. Voitkiv and N. Grün, J. Phys. B **34**, 267 (2001).

[57] B. Najjari, A. Surzhykov, and A. B. Voitkiv, Phys. Rev. A **77**, 042714 (2008).

[58] F. Drepper and J. S. Briggs, J. Phys. B **9**, 2063 (1976).

[59] H.-P. Hülskötter, B. Feinberg, W. E. Meyerhof, A. Belkacem, J. R. Alonso, L. Blumenfeld, E. A. Dillard, H. Gould, N. Guardala, G. F. Krebs, M. A. McMahan, M. E. Rhoades-Brown, B. S. Rude, J. Schweppe, D. W. Spooner, K. Street, P. Thieberger, and H. E. Wegner, Phys. Rev. A **44**, 1712 (1991).

[60] A. Belkacem, H. Gould, B. Feinberg, R. Bossingham, and W. E. Meyerhof, Phys. Rev. A **56**, 2806 (1997).

[61] N. Claytor, A. Belkacem, T. Dinneen, B. Feinberg, and H. Gould, Phys. Rev. A **55**, R842 (1997).

[62] T. Stöhlker, D. Ionescu, P. Rymuza, T. Ludziejewski, P. Mokler, C. Scheidenberger, F. Bosch, B. Franzke, H. Geissel, O. Klepper, C. Kozhuharov, R. Moshammer, F. Nickel, H. Reich, Z. Stachura, and A. Warczak, Nucl. Instrum. Methods Phys. Res. B **124**, 160 (1997).

[63] C. Scheidenberger and H. Geissel, Nucl. Instrum. Methods Phys. Res. B **135**, 25 (1998).

[64] H. F. Krause, C. R. Vane, S. Datz, P. Grafström, H. Knudsen, C. Scheidenberger, and R. H. Schuch, Phys. Rev. Lett. **80**, 1190 (1998).

[65] K. Momberger, N. Grün, W. Scheid, and U. Becker, J. Phys. B **22**, 3269 (1989).

[66] G. Deco, K. Momberger, and N. Grün, J. Phys. B **23**, 2091 (1990).

[67] J. Ullrich, R. Moshammer, A. Dorn, R. Dörner, L. P. H. Schmidt, and H. Schmidt-Böcking, Rep. Prog. Phys. **66**, 1463 (2003).

[68] H. Kollmus, R. Moshammer, R. E. Olson, S. Hagmann, M. Schulz, and J. Ullrich, Phys. Rev. Lett. **88**, 103202 (2002).

[69] R. Moshammer, W. Schmitt, J. Ullrich, H. Kollmus, A. Cassimi, R. Dörner, O. Jagutzki, R. Mann, R. E. Olson, H. T. Prinz, H. Schmidt-Böcking, and L. Spielberger, Phys. Rev. Lett. **79**, 3621 (1997).

[70] A. B. Voitkiv, Phys. Rev. A **72**, 062705 (2005).

[71] A. B. Voitkiv, B. Najjari, and J. Ullrich, Phys. Rev. Lett. **92**, 213202 (2004).

[72] A. B. Voitkiv and B. Najjari, Phys. Rev. A **79**, 022709 (2009).

[73] H. Reich, W. Bourgeois, B. Franzke, A. Kritzer, and V. Varentsov, Nucl. Phys. A **626**, 417 (1997).

[74] O. Jagutzki, A. Cerezo, A. Czasch, R. Dörner, M. Hattas, M. Huang, V. Mergel, U. Spillmann, K. Ullmann-Pfleger, T. Weber, H. Schmidt-Böcking, and G. Smith, IEEE Trans. Nucl. Sci. **49**, 2477 (2002).

[75] O. Klepper and C. Kozhuharov, Nucl. Instrum. Methods Phys. Res. B **204**, 553 (2003).

[76] S. Trotsenko, T. Stöhlker, D. Banas, C. Z. Dong, S. Fritzsche, A. Gumberidze, S. Hagmann, S. Hess, P. Indelicato, C. Kozhuharov, M. Nofal, R. Reuschl, J. Rzadkiewicz, U. Spillmann, A. Surzhykov, M. Trassinelli, and G. Weber, J. Phys.: Conf. Ser. **58**, 141 (2007).

[77] C. Z. Dong, D. H. Zhang, T. Stöhlker, S. Fritzsche, and B. Fricke, J. Phys. B **39**, 3121 (2006).

[78] N. Petridis, A. Kalinin, U. Popp, V. Gostishchev, Y. Litvinov, C. Dimopoulou, F. Nolden, M. Steck, C. Kozhuharov, D. Thorn, A. Gumberidze, S. Trotsenko, S. Hagmann, U. Spillmann, D. Winters, R. Dörner, T. Stöhlker, and R. Grisenti, Nucl. Instrum. Methods Phys. Res. A **656**, 1 (2011).

[79] G. Rodrigues, P. Indelicato, J. Santos, P. Patté, and F. Parente, At. Data. Nucl. Data Tables **86**, 117 (2004).

[80] B. Najjari and A. B. Voitkiv, Phys. Rev. A **85**, 052712 (2012).

[81] B. Najjari and A. B. Voitkiv, Phys. Rev. A **87**, 034701 (2013).

[82] S. Fritzsche (unpublished).

[83] K. T. Cheng, M. H. Chen, and W. R. Johnson, Phys. Rev. A **77**, 052504 (2008).